Appendix B

Supporting Papers

This appendix contains the text of five conference papers which were published during the course of the research. All were co-authored by Prof. W.H. Melbourne.

1. Pages **B–2** to **B–9**: 'Measurement of sectional lift forces on an oscillating cylinder', published in the proceedings of the *Second Asia-Pacific Conference on Wind Engineering*, Beijing University, June 1989.

2. Pages **B–10** to **B–11**: 'Frequency and time domain cancellation of inertial signal from an accelerating force transducer', presented to the *Workshop on Industrial Fluid Dynamics, Heat Transfer and Wind Engineering*, CSIRO Division of Building, Construction and Engineering, Melbourne, December 1989.

3. Pages **B–12** to **B–15**: 'Measurements of coefficients of lift and spanwise correlation for a circular cylinder oscillating in a turbulent flow', presented to the *Tenth Australasian Fluid Mechanics Conference*, University of Melbourne, December 1989.

4. Pages **B–16** to **B–18**: 'Promotion of instability during lock-in', presented to the *Australian Wind Engineering Society Seminar: Wind engineering for the 90s*, Polkolbin, NSW, February 1991.

5. Pages **B–19** to **B–30**: 'Lift on an oscillating cylinder in smooth and turbulent flow', presented to the *Eighth International Conference on Wind Engineering*, University of Western Ontario, July 1991.

MEASUREMENT OF SECTIONAL LIFT FORCES ON AN OSCILLATING CYLINDER

H.M. Blackburn and W.H. Melbourne
Department of Mechanical Engineering, Monash University, Australia.

ABSTRACT An experimental method is presented for the measurement of lift forces and coherence on a vibrating cylinder in transcritical turbulent flow. The force measurements were made on six sections of a cylinder and the method by which the inertial component of the load signal was removed is described. Timeseries of lift forces on rigid and vibrating cylinders at subcritical and critical Reynolds Numbers are presented.

1. Introduction

The response prediction of chimneys in turbulent air flow depends upon an understanding of the vortex-shedding process and lock-in. Specifically this requires knowledge of the magnitude and coherence of the fluctuating lift forces acting on an oscillating cylinder over a range of Reynolds Numbers in turbulent flow. A method has been developed of measuring cross-flow forces acting on short sections of a circular cylinder undergoing forced sinusoidal oscillations in a wind tunnel. A critical aspect of these measurements compared to those made before is that aerodynamic forces are measured simultaneously on six short segments of the cylinder, so that changes in correlation length can be observed as amplitude of oscillations increase. In this paper the equipment and the computational methods used will be described, and sample results in the form of aerodynamic force timeseries for a rigid and a vibrating cylinder in smooth flow will be presented.

2. Equipment

2.1 Wind tunnel model

In the experimental programme, cross-flow aerodynamic loads were measured on short (0.1 diameter) sections of a smooth circular cylinder which could be forced into harmonic motion at amplitudes up to 0.03 diameter.

The part of the equipment exposed to the flow is a 200mm diameter, 900mm long circular cylinder. A sketch of the cylinder installed in the

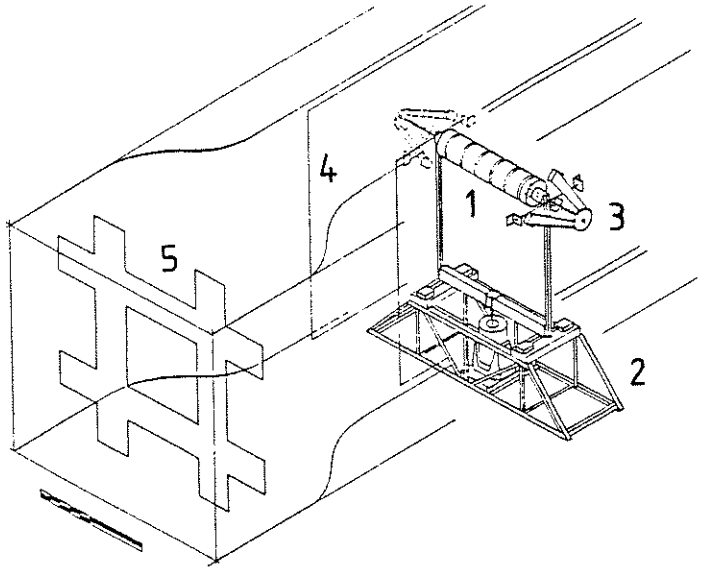

Figure 1: Sketch of cylinder installed in wind tunnel. **1**: Cylinder with 6 force transducers; **2**: Support truss, yoke, electromagnetic shaker, beam springs; **3**: Wire support harness; **4**: End plates; **5**: Turbulence grid.

2m×1m working section of the Monash University 400kW wind tunnel is shown in Figure 1. Six force transducer shells are mounted in each measurement section as part of the cylinder, equispaced along the axis. The cylinder is supported on a structural yoke which passes through the inside of the cylinder, through the tunnel walls, then extends down below the tunnel. The yoke is mounted on beam springs atop a trussed structure which also holds a 450N electromagnetic shaker. The yoke is guided by a wire restraint harness which resists the drag forces, prevents axial movement and supresses undesirable vibration modes. The cylinder thus constrained can only move up and down, driven by the shaker at the natural frequency of cylinder-yoke assembly on the beam springs. The frequency can be adjusted by changing the length or stiffness of the springs.

There are two large end plates reaching from the floor to the roof of the wind tunnel, extending 2.5 diameters upstream and 4.5 diameters downstream of the cylinder centreline. The gap of 3mm between each end of the cylinder and the plates is effectively sealed using synthetic fur, while freedom of movement is retained.

2.2 Transducers

The transducers consist of very light, stiff cylindrical shells of composite construction which distribute aerodynamic load to four cantilever beam

springs. The springs are mounted on a central ring which clamps onto the structural inner cylinder; each beam has a semiconductor strain gauge glued to it, thus providing a full strain bridge. On the central ring is also mounted an accelerometer, so that the cross-flow acceleration (hence velocity and displacement) can be measured. The accelerometer provides output to enable the cancellation of the part of the strain bridge signal due to the mass of the outer shells, as described in Section 3.

2.3 Remainder of construction

The construction of the remainder of the cylindrical shape (between the force measurement transducers) uses thin plywood, balsawood and fibreglass to minimize weight. The outer surface of the cylinder was rubbed back to a smooth finish. The maximum deviation from circular shape measured at any section on the assembled cylinder was 0.2mm — 0.001 diameter; the average maximum deviation was 0.14mm.

Gaps of 0.5mm to 0.8mm between the force measurement transducers and the aerodynamic shells remained after assembly; these were sealed using strips cut from latex condoms, stretched and glued in place. The stretched thickness of the latex material was about 0.03mm.

3. Data Processing

3.1 The basis of the method

The method used for extracting that part of the transducer signal due to aerodynamic force on each section is based on the fact that the force sensed by the transducer should just be the sum of the aerodynamic force acting on it and the inertial force caused by the acceleration of the cylinder and the mass of the light, spring-mounted cylindrical shell sections. This inertial force should be highly coherent with the output signal of the accelerometer mounted at each station, and so can be estimated either in the time domain using the impulse response function of the transducer to acceleration, or in the frequency domain using the frequency response function of the transducer to acceleration, in conjunction with the signal from each accelerometer. Thus the inertial force can be computed and subtracted from the total leaving the aerodynamic component. It was decided to do the computations of the acceleration-coherent part of the force in the frequency domain, making extensive use of FFT-based techniques.

This method requires that estimates of the frequency response function between cylinder acceleration and transducer output be available. These were computed from timeseries recorded in the absence of airflow, while the cylinder was excited by broadband random noise by the electromagnetic shaker

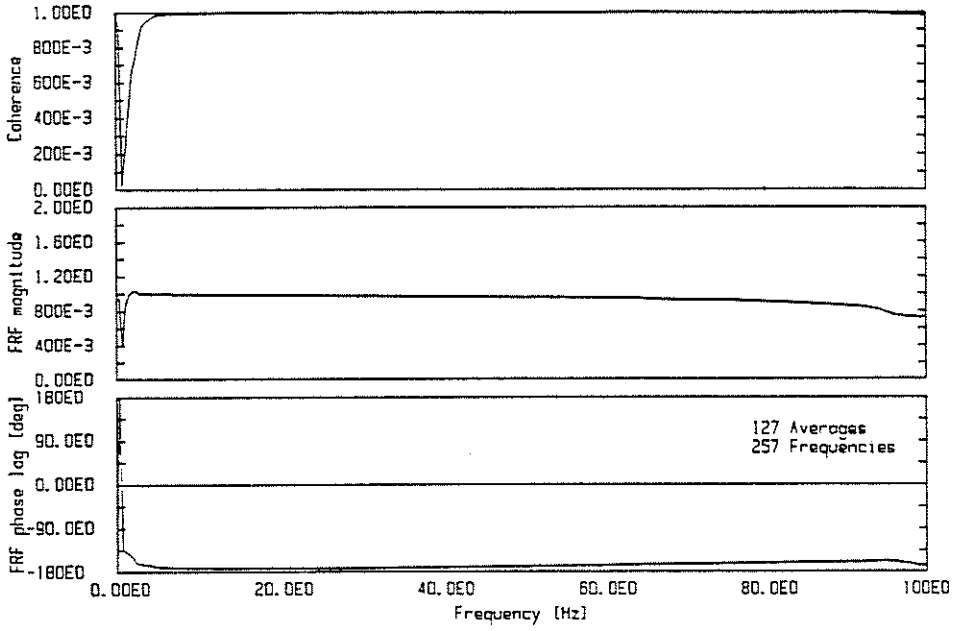

Figure 2: Force transducer frequency response function to acceleration.

mounted underneath the wind tunnel. To remove the influence of the added mass of the surrounding fluid in the results of the frequency response function estimation, thin plastic shields were wrapped around the cylinder at each transducer location during this phase of the experiment. The frequency response function estimates for each transducer are used as look-up tables later in the computational technique. A typical example of such a frequency response function estimated from recorded timeseries using standard digital procedures is shown in Figure 2.

3.2 Data recordings

The output from all six transducers mounted in the cylinder were recorded at the same time by 12-channel data collection on one of the Department's Perkin-Elmer minicomputers. A typical data collection is 8192 records long, sampling rate 200Hz, thus allowing sufficient data for meaningful averages to be extracted after processing is done.

3.3 Dynamic calibration of transducers

To check that the procedures employed could in fact recover estimates of external force in the presence of shaking of the cylinder, a dynamic calibration method was used. A load-beam of comparatively low stiffness and mass was made and strain gauges attached, so that it could also act as a force transducer. After static calibration of this load-beam, it was mounted

underneath each transducer in turn so that it applied an external load to the transducer, and the electromagnetic shaker was switched on, thus forcing the cylinder to vibrate on the load-beam.

Using a similar procedure to that outlined in Section 3.1, the acceleration-coherent part of the total tranducer signal was removed and the remainder was fitted to the output of the load-beam strain bridge amplifier using a multiplicative calibration constant determined by the method of linear least-squared error. This constant is made available to the correction and calibration procedures carried out in the main processing. Agreement between the predicted and measured force signals was good.

4. Experimental Results

4.1 Range of results presented

The results presented here are corrected and calibrated aerodynamic force, measured in Newtons, for smooth flow tests conducted on a rigid cylinder and a cylinder undergoing forced harmonic vibrations. Only 201 points out of the total 8192 collected for each channel are displayed.

4.2 Fixed base timeseries

For this experiment, the cylinder support yoke was clamped to the supporting structure to rigidly fix the cylinder. Figures 3(a) & (b) show corrected force timeseries at blockage corrected Reynolds Numbers of 1.41×10^5 and 4.80×10^5 respectively.

In Figure 3(a) the flow is clearly subcritical, as evidenced by the narrow band vortex shedding which had a centre frequency of 9.3Hz. Note that the vortex-shedding is not completely coherent along the length of the cylinder, with the phase of shedding at each station changing a small amount, apparently at random. The average computed R.M.S. Coefficient of Lift was 0.44, while the Strouhal Number was 0.18.

In Figure 3(b) the flow has made the transition to the range of critical Reynolds Numbers, and the cross-flow processes are much more wide- banded than before, with no discernable spectral peak. The R.M.S. Coefficient of Lift was 0.10.

4.3 Vibrating cylinder

For the data shown in Figures 4(a) & (b) , the cylinder was forced to oscillate at a frequency of 25.5Hz, with an peak-to-peak amplitude of 2.25% of diameter. The blockage corrected Reynolds Numbers are 1.45×10^5 and 4.75×10^5 respectively.

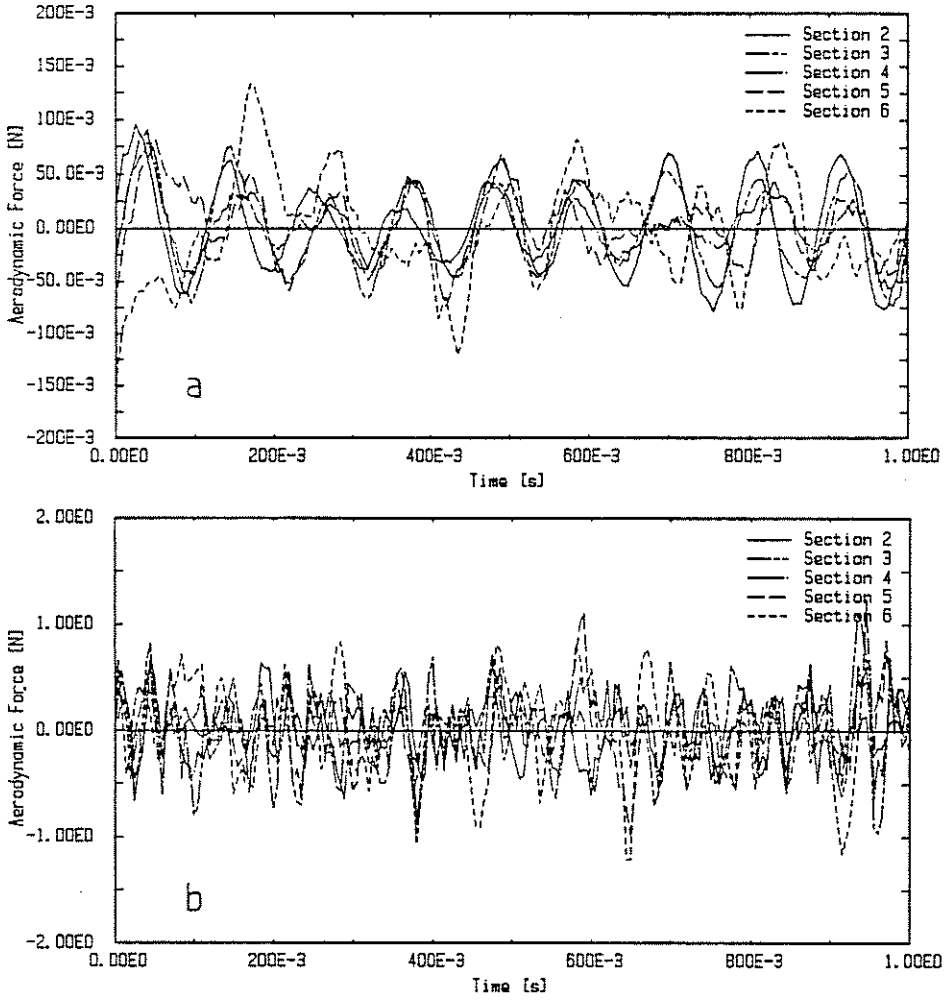

Figure 3: Force timeseries measured on a rigid cylinder at Reynolds Numbers (a) 1.4×10^5 and (b) 4.8×10^5.

Figure 4(a), with the Reynolds Number close to that for the data used in Figure 3(a), again exhibits subcritical flow, with a vortex-shedding centre frequency of 9.7Hz, however significant energy also appears at the first and third harmonics of the shaking frequency. Otherwise the data appear similar to those presented in Figure 3(a), for the fixed-base case. The R.M.S. Coefficient of Lift was 0.50, and the Strouhal Number was 0.18.

The data of Figure 4(b) likewise show critical flow with broadbanded force signals, and as in Figure 4(a) there are significant spectral peaks at the first and third harmonics of the shaking frequency. The R.M.S. Coefficient of Lift was 0.11.

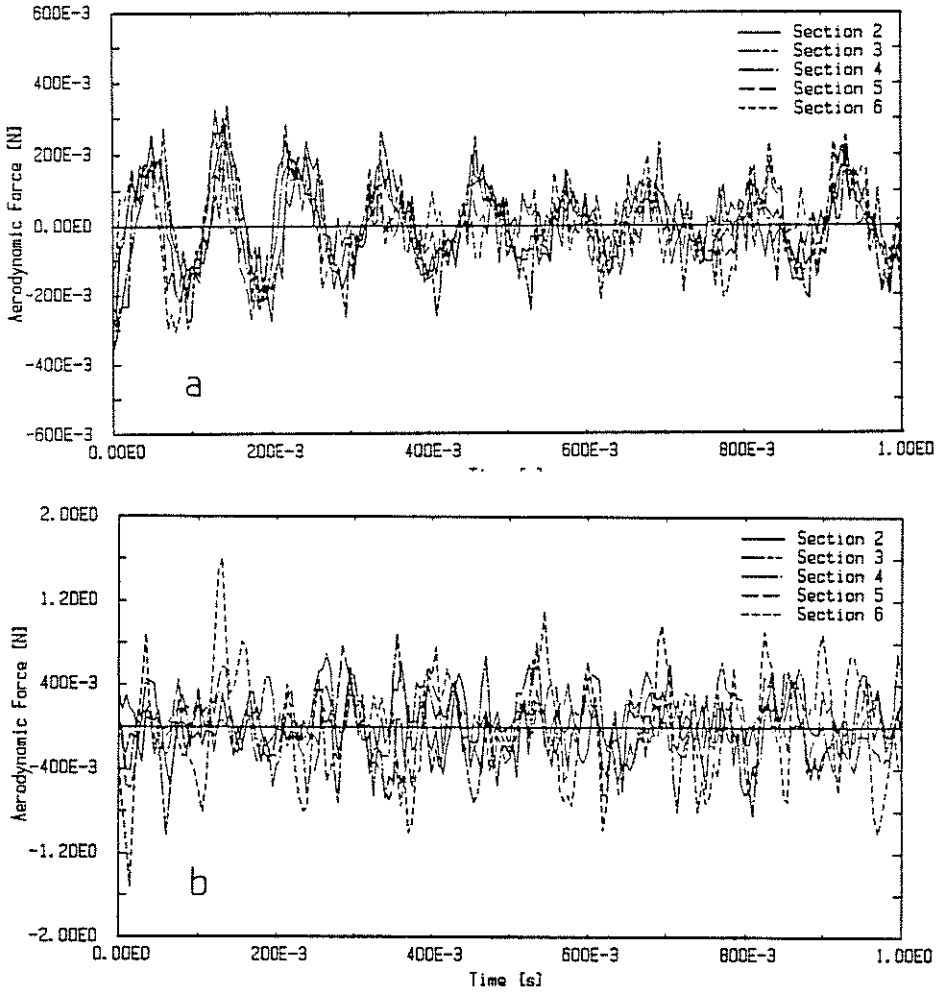

Figure 4: Force timeseries measured on a vibrating cylinder at Reynolds Numbers (a) 1.4×10^5 and (b) 4.8×10^5.

An autospectrum of one of the channels of Figure 4(b) is shown as Figure 5. The broadband nature of the cross-flow force can be clearly seen, as can spectral peaks at the first and third harmonics of the shaking frequency.

5. Conclusions

The experimental method described has been shown capable of measuring aerodynamic force at six subsections of a fixed or vibrating circular cylinder simultaneously. It is possible that some residual errors exist in the estimated forces near the shaking frequency of the cylinder, since the method is not capable of acheiving complete accuracy in the absence of flow, however the residue is small. The relative size of the aeroelastic component of force at

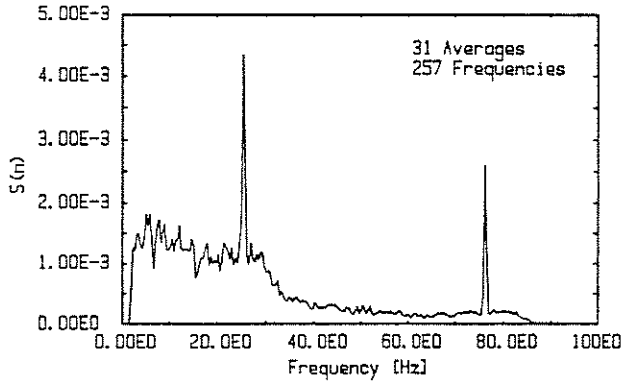

Figure 5: Autospectrum of force transducer timeseries of data used for Figure 4(b). Note the spectral peaks at the shaking frequency and its third harmonic.

the third harmonic of the shaking frequency was surprising, and has not been commented on before in the literature. This is not an artifact of the data processing (which is inherently linear in any case), since the third harmonic component is also present in the raw data.

The data presented for R.M.S. Coefficient of Lift and Strouhal Number for the rigid cylinder compare favourably with those presented by Cheung & Melbourne [1]. For instance, at the lower Reynolds Number of 1.41×10^5, they report R.M.S. Coefficient of Lift as 0.41, compared with 0.44 here. At Reynolds Number 4.8×10^5 their R.M.S. Coefficient of Lift is 0.05, comparing in this case with 0.10. It is to be expected that lift coefficients measured at sections (length 0.1 diameter) should be greater than those over the whole cylinder, as per Cheung & Melbourne's measurements (length approximately 5 diameters), particularly in the critical Reynolds Number regime where the spanwise coherence is lower. The value of Strouhal Number of 0.18 at the lower Reynolds Number in these experiments compares well with theirs of 0.19.

In future work the range of parameters investigated will be extended, with particular emphasis on turbulent flow at Reynolds Numbers up to 6×10^5, and aeroelastic coefficients will be computed.

Reference

[1] CHEUNG J.C.K. & MELBOURNE W.H. Turbulence effects on some aerodynamic parameters of a circular cylinder at supercritical Reynolds Numbers *Jnl. Wind Eng. and Indust. Aero.* **14** (1983) pp 393 – 410.

Frequency and Time Domain Cancellation of Inertial Signal from an Accelerating Force Transducer

H.M. Blackburn
W.H. Melbourne
Department of Mechanical Engineering
Monash University, Clayton 3168, Australia

Measuring the unsteady fluid forces acting on an oscillating structure usually entails some correction of force transducer output to account for the inertial component of the response due to the mass and acceleration of the sensor element. In the application discussed here, the interaction between structural oscillation and cross flow vortex shedding forces acting on a circular cylinder in wind tunnel flow is being studied. Short (0.1 diameter axial length) segments of the cylinder are mounted from an inner structural tube on stiff beam springs which have strain gauges bonded to them in a full bridge circuit. The mechanical arrangement of the springs and gauges provides a sensor element which is only sensitive to cross-flow force. The cylinder can be forced to oscillate in a cross flow direction at amplitudes of up to 6% of diameter peak-to-peak.

The sections of the cylinder which distribute force to the four beam springs have been made as light as possible, consistent with the need for internal stiffness, by use of fibre-composites, foamed plastics and balsa wood. The sensor elements have a finished mass of 16gm for a 20mm long segment of a 200mm diameter cylinder. The natural frequency of the sensor segments on their spring mounts is about 400Hz. Despite the attention given to weight reduction, the magnitude of sensor response to acceleration when oscillating is of the order of 10 times larger than response to aerodynamic force, so that some means must be applied to cancel the inertial signal.

Various methods have been used to address this measurement problem in the past. Historically the first was mechanical cancellation of inertial signal, with another mass attached to the oscillating structure via strain-gauged springs. The response of this sensor was adjusted until it cancelled the inertial component of the aerodynamic sensor response at the frequency of interest. A second method employed was analogue electronic, with the input to the cancellation circuit coming from an accelerometer attached to the structure. This method also needed adjustment of system parameters, either electronically or by the operator, to give correct cancellation.

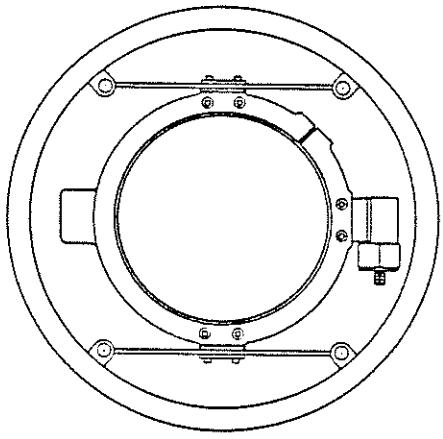

Figure 1: End view of force transducer station, showing beam springs, cylinder segment, and accelerometer.

The more recent development of digital signal processing techniques has made possible new approaches to the problem. In the present application, an accelerometer is placed at each transducer station to provide a signal from which a cancellation signal can be derived. The signal processing problem is then one of *identification*, that is, modelling the relationship between accelerometer signal and force transducer signal in the ab-

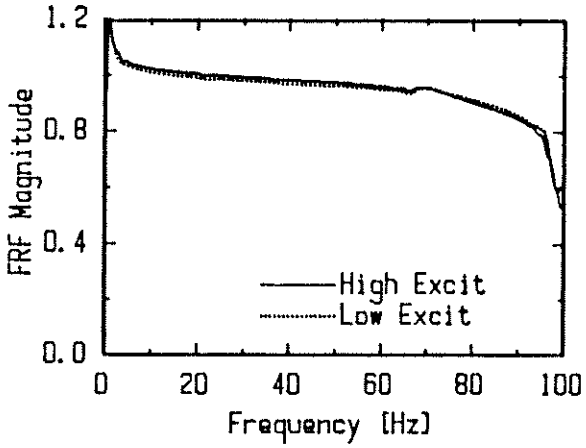

Figure 2: Transducer FRF magnitude for acceleration input, showing small variation with excitation level.

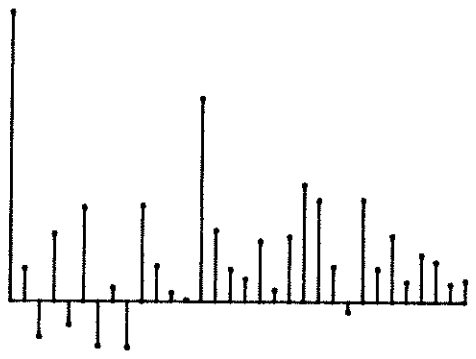

Figure 3: Transducer impulse response, fitted using recursive least squared error techniques.

sence of flow. This relationship can be used to predict the inertial component of signal given the output from the accelerometer.

Two methods have been tried. In the first, the frequency response function (FRF) of the force tranducer to acceleration is estimated in the absence of flow using random vibration input to the structure, recording a long timeseries of the two transducer responses, and using FFT-based frequency domain procedures to estimate the transducer FRF. The inertial component of transducer signal is estimated by transforming recorded timeseries into the frequency domain and multiplying the Discrete Fourier Transforms of the accelerometer signal and the transducer FRF. The product is subtracted from the DFT of the force transducer output and the remainder is transformed back to the time domain to give an estimate of the force transducer response to aerodynamic force alone. The method works reasonably well, but suffers from the difficulty that the transducers have slightly nonlinear characteristics when assembled. This is reflected in the fact that the FRF estimates can differ by a few percent when the level of excitation is varied (Figure 2). Attempts to overcome this by multiplying the input timeseries of the force transducer by an inverse nonlinear function before further processing achieves some improvement in cancellation but the results are not entirely satisfactory.

A second method has more recently been developed, in which the impulse response function (IRF) of the force transducer to acceleration is estimated in the time domain using recursive least squared error procedures (Figure 3). The IRF is then convolved with the accelerometer timeseries recorded with the flow on to produce an estimate of the inertial response. This method has the practical advantage that the length of timeseries needed to produce a satisfactory estimate is much shorter than that needed for the frequency domain procedures previously discussed, so that short records of response to acceleration can be taken in the absence of flow before each run. The fact that these can be recorded while the cylinder is oscillating at the amplitude and frequency of interest also effectively overcomes the problems of nonlinear transducer characteristics and any drift in characteristics of the apparatus with temperature.

Comparison of the two methods shows the time domain modelling to be more successful, both in practical terms and in size of errors as assessed by examining the timeseries of residual force transducer output recorded in the absence of flow. The size of the RMS error achieved using the frequency domain correction method is of the order of ten analogue-to-digital digitization increments, while that of the time domain method is typically of the order of one digitization increment (the theoretical minimum).

MEASUREMENTS OF COEFFICIENTS OF LIFT AND SPANWISE CORRELATION FOR A CIRCULAR CYLINDER OSCILLATING IN A TURBULENT FLOW

H.M. Blackburn and W.H. Melbourne
Department of Mechanical Engineering
Monash University, Clayton, Vic. 3168, AUSTRALIA

ABSTRACT

For structures such as chimney stacks in the atmospheric boundary layer, measurements of cross-flow aerodynamic forces at high Reynolds Numbers and low response amplitudes are needed before more accurate models for structural response can be developed.

A prediction technique has been developed for the measurement of cross-flow forces acting on six short sections of a cylinder undergoing forced sinusoidal oscillations in a wind tunnel. Aerodynamic lift forces measured using this technique are decomposed into terms corresponding to aerodynamic damping, added mass and a residual random component. These measurements can then be used in the prediction of structural response.

Measurements of lift forces from a cylinder oscillating in a turbulent flow of 4% intensity at a Reynolds Number of 1.7×10^5 are presented. Oscillation amplitudes vary up to 3% of diameter and Reduced Velocity between 4 and 6. The results indicate that varying the oscillation amplitude and Reduced Velocity in this range has an effect on aerodynamic damping but that the residual forces are unaffected by the motion, both locally at each measurement position and in spanwise correlation.

INTRODUCTION

The prediction of cross-flow response of slender circular cylindrical structures to vortex shedding is still a relatively inaccurate process. This is due partly to a lack of understanding of the vortex shedding process itself and in particular the interaction of structural and fluid oscillations and also a lack of measurements of critical aerodynamic data.

When the amplitude of structural oscillation is very small the structural response is of a narrow banded random nature and prediction of response amplitudes may be carried out using random vibration techniques such as those presented by Vickery and Clark (1972). As the oscillations of the structure increase in amplitude, particularly when the structural frequencies and vortex shedding frequencies coincide, there is an interaction between the structural and fluid oscillations and the aerodynamic forces can increase dramatically. Data presented by Jones (1968) and Sarpkaya (1978), have shown that this interaction can occur in smooth flows at amplitudes of a few percent of diameter.

If the relative mass and structural damping of the structure are very low the cross-flow amplitudes can become of the same order as the cylinder diameter and the response timeseries becomes very narrow-banded, approaching a sinusoidal waveform. In this case Sarpkaya (1978) suggested that the response parameter Sq may be used to derive an estimate of the response amplitude.

In the middle ground where the response amplitudes are small and the fluid forces and structural response are still of a random nature but there is significant interaction between the flow and structural oscillations, comparatively few engineering models exist that enable the prediction of response amplitudes. One significant model for this regime is that provided by Vickery and Basu (1983), which is essentially that of Vickery and Clark (1972) but altered to include an aerodynamic damping term which depends non-linearly on response amplitude, however at low amplitudes the effect is predominantly linear. Inherent in this model is the assumption that the interaction between the structural and fluid motion is entirely incorporated in the aerodynamic damping term, which implies motion-dependent forces which are fully correlated in the spanwise direction. The remaining aerodynamic forces producing random structural vibration are supposed to be unaffected by the structural response amplitude.

In order to investigate the influence of cross-flow oscillation on aerodynamic forces due to vortex shedding, a wind-tunnel model was manufactured which enables forces to be measured simultaneously at several sections of a circular cylinder while the cylinder is forced to oscillate in a cross-flow direction. From the recorded timeseries of forces estimates of aerodynamic damping and mass can be extracted by correlating aerodynamic forces with the velocity and acceleration of the structure, leaving forces which are uncorrelated with cylinder motion.

In this paper experimental results are presented which demonstrate negative aerodynamic damping at vibration amplitudes of 3% of diameter and below at a Reynolds Number just at the start of the critical regime in a turbulent flow of 4% streamwise intensity. The parts of aerodynamic force which are uncorrelated with the motion of the cylinder are shown to be unaffected by the motion, both locally and in spanwise correlation.

EXPERIMENTAL TECHNIQUE

A sketch showing the general arrangement of the wind tunnel model is presented in Figure 1. The cylinder is 200mm diameter with an aspect ratio of 4.5. There are six force measurement transducers each supporting a section of cylinder 0.1 diameter long, spaced equally along the cylinder axis with a spacing of 0.75 diameter. Narrow air-gaps between the sections of cylinder are sealed with thin polyurethane elastomer. To mount the cylinder sections each transducer contains four beam springs with bonded semi-conductor strain gauges. The beams are aligned so that cross-flow forces induce bending stresses in the springs. An accelerometer which measures cross-flow acceleration is also contained at each transducer station. The cylinder can be forced to oscillate in a direction normal to the flow by an electromagnetic shaker at a maximum amplitude of 3% of diameter (6% peak-to-peak).

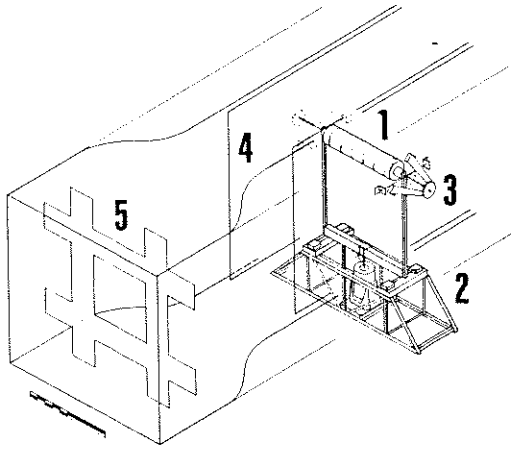

Figure 1 Sketch of cylinder installed in wind tunnel. **1**: Cylinder with 6 force transducers; **2**: Support truss, yoke, electromagnetic shaker, beam springs; **3**: Wire support harness; **4**: End plates; **5**: Turbulence grid.

When the cylinder is oscillating, the force measured by each transducer contains a component due to aerodynamic force and a component due to the mass and acceleration of the section of cylinder supported by the transducer. DFT-based techniques are used to extract the aerodynamic portion of the measured forces, using simultaneous records of force transducer and accelerometer outputs together with experimentally-determined estimates of the frequency response functions of the transducers to acceleration. Details of the experimental apparatus and data processing have been presented by Blackburn and Melbourne (1989).

The aerodynamic forces computed to act at each measurement station can be further processed by extracting components which are correlated with cylinder cross-flow velocity and acceleration on a least-squares basis. Since velocity and acceleration are uncorrelated in harmonic motion, the components thus extracted are also mutually uncorrelated. These components of motion-correlated force correspond to aerodynamic damping and added mass forces.

RESULTS

The aerodynamic force data presented here were collected in a turbulent flow at a blockage-corrected Reynolds Number of 1.7×10^5. The turbulence of 4% longitudinal intensity and an integral length scale of 1.5 diameters was produced by a turbulence grid located 50 cylinder diameters upstream of the model.

A comparison of cross-flow force autospectra at a Reynolds Number of 1.7×10^5 is shown in Figure 2.

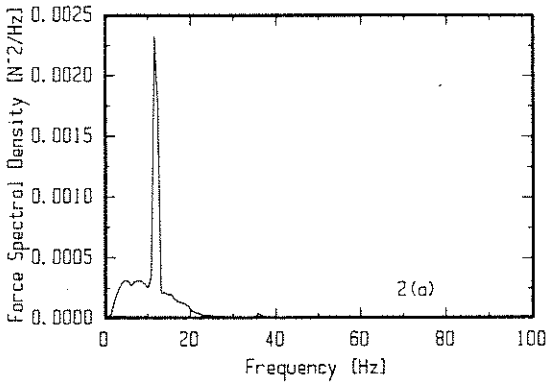

Figure 2(a) Autospectrum of cross-flow aerodynamic forces measured at one force transducer with the cylinder in forced oscillation at 3% of diameter amplitude.

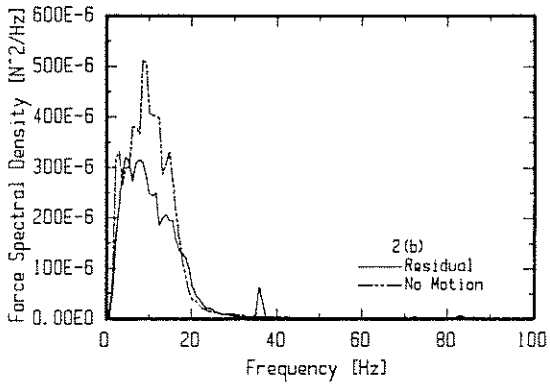

Figure 2(b) Comparison of spectra of residual cross-flow forces after removal of motion-correlated forces and forces recorded in the absence of shaking.

In Figure 2(a) the cylinder is driven by the shaker to an amplitude of 3% of diameter at a frequency of 12 Hz; the presence of aerodynamic forces at the shaking frequency can be clearly seen. Figure 2(b) shows the spectrum of the same data used to generate Figure 2(a) but after removal of terms correlated with motion, together with a spectrum recorded at the same Reynolds Number with the cylinder held fixed. In the spectrum of residual forces, the sharp peak at the shaking frequency has been removed but there is still some energy there. Also of interest is the presence of components at the third harmonic of the shaking frequency. Higher harmonics are not removed by the correlation process since they

are orthogonal to the first harmonic and hence uncorrelated with it. When the cylinder is held stationary the other spectrum of Figure 2(b) shows that the vortex shedding process is quite wide-banded at Reynolds Number 1.7 x 10^5, but with a distinct spectral peak at 9 Hz (Strouhal Number = 0.14). Comparing the two spectra of Figure 2(b), introduction of shaking causes the distinct peak at 9 Hz to disappear and the residual R.M.S. lift to forces drop slightly. However raising the Reynolds Number to 1.8 x 10^5 in the absence of shaking also caused the distinct peak at 9 Hz to disappear, indicating that boundary layer effects are just bringing on the transition to critical flow, making the lift forces sensitive to small variations in Reynolds Number.

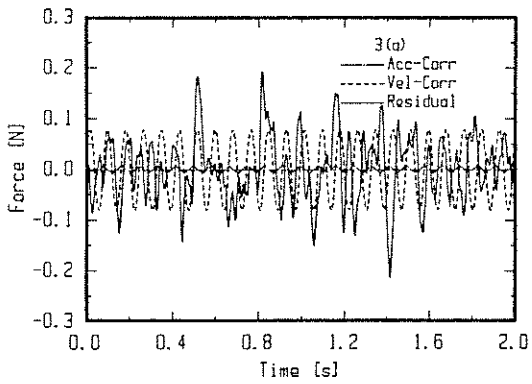

Figure 3(a) Plot of force components decomposed into those correlated with motion, and residual.

Typical force timeseries from which spectra and Coefficients of Lift are prepared are illustrated in Figures 3(a) and (b). Figure 3(a) indicates the relative sizes of the acceleration-correlated, velocity-correlated and residual force terms at 3% of diameter amplitude. Figure 3(b) shows timeseries of force before and after removal of motion-correlated terms.

Coefficients of Lift can be prepared from the force timeseries decomposed as previously described. Figure 4 shows the Coefficients of Lift of the residual forces from one of the force measurement rings at amplitudes of 1%, 2% and 3% of diameter as functions of Reduced Velocity.

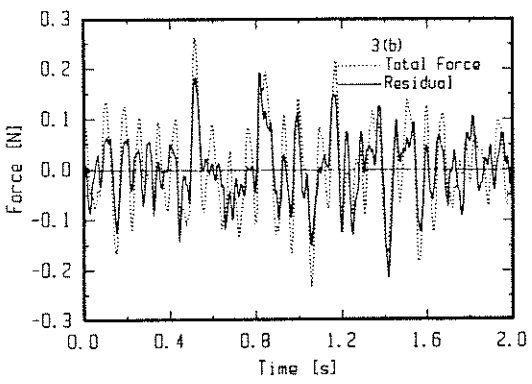

Figure 3(b) Comparison of aerodynamic forces before and after removal of motion-correlated terms.

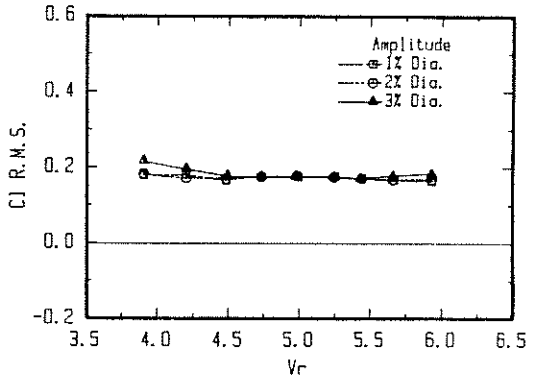

Figure 4. R.M.S. Coefficients of Lift from forces uncorrelated with motion as functions of Reduced Velocity and amplitude. The R.M.S. C_l at the same Reynolds Number for no motion is 0.21.

Magnitudes of Coefficient of Lift of uncorrelated forces for the four most central transducers are all of a similar magnitude although there is some variation from ring to ring, as shown in Figure 5. All the Coefficients of Lift of residual forces display the same relative independence of Reduced Velocity.

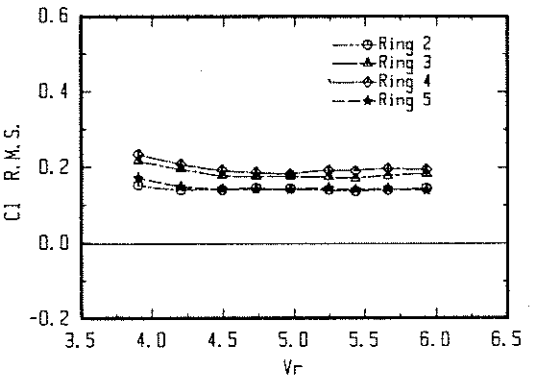

Figure 5 R.M.S. Coefficients of Lift from forces uncorrelated with motion at 3% of diameter amplitude. Comparison of results from four most central transducers.

The Coefficients of Lift of the velocity-correlated forces at 3% of diameter amplitude are shown in Figure 6. These forces correspond to aerodynamic damping: a positive value of Coefficient of Lift indicates negative aerodynamic damping, that is the flow is transferring energy to the structure. Coefficients measured at lower amplitudes show the same trends.

The Coefficients of Lift of the acceleration-correlated forces at the same amplitude are shown in Figure 7. These forces correspond to Added Mass of fluid: a positive value of Coefficient of Lift indicates a negative added mass.

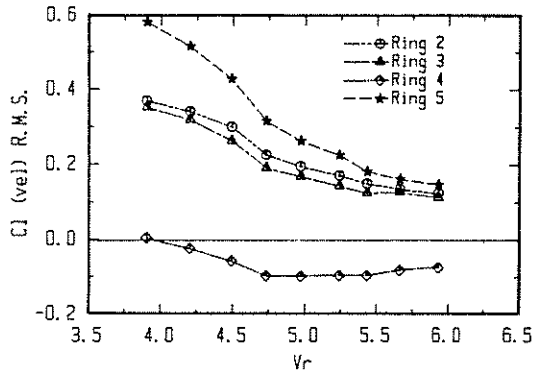

Figure 6. Velocity-correlated R.M.S. Coefficients of Lift measured at four transducers as functions of Reduced Velocity at 3% of diameter amplitude.

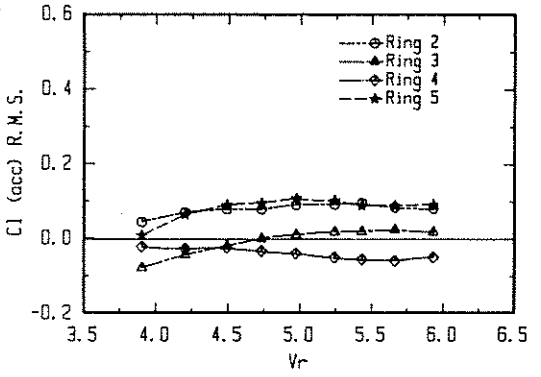

Figure 7. Acceleration-correlated R.M.S. Coefficients of Lift measured at four transducers as functions of Reduced Velocity at 3% of diameter amplitude.

The signs of the motion-correlated Coefficients of Lift and their trends with Reduced Velocity correspond broadly with those found by other workers, for example Sarpkaya (1978) who conducted forced oscillation experiments in subcritical flow. It seems from an inspection of Figures 6 and 7 that there is an offset in mean value between the Coefficients of Lift found at each of the four central force measurement stations, but a similar trend with Reduced Velocity for each. At this stage it is uncertain if this effect is due to experimental error or aerodynamic effects caused perhaps by spanwise variation in boundary layer flows at the onset of the critical Reynolds Number regime.

While motion-dependent forces are by definition perfectly correlated in a spanwise direction although perhaps with a variation in sign, the residual forces show a reducing degree of coherence in the spanwise direction as the measurement stations become further apart, as has been known for some time. From cross-correlations computed between the aerodynamic forces at the various locations plots have been prepared. Although of limited spanwise resolution, they can still be used to compare the spanwise correlation of residual aerodynamic force as a function of oscillation amplitude. Figure 8 indicates that there was no observable change in spanwise correlation with increase of oscillation amplitude.

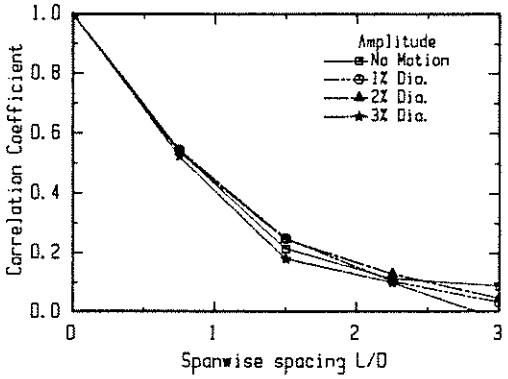

Figure 8. Plot of spanwise correlation of residual force as a function of amplitude at Reduced Velocity of 5.25.

CONCLUSION

The experimental results indicate that in the flow regime investigated, cross-flow oscillation has little influence on the portion of the aerodynamic forces which are not correlated with the motion of the structure, both locally and in spanwise correlation.

Analysis of motion correlated forces suggests that a negative aerodynamic damping exists and varies with Reduced Velocity in a manner broadly similar to studies conducted both in subcritical [Sarpkaya (1978)] and postcritical [Jones (1980)] smooth flows.

There is agreement between experimental results and Vickery and Basu's (1983) model in that there was no observed interaction between motion and uncorrelated local forces and spanwise correlation.

REFERENCES

BLACKBURN, H.M. and MELBOURNE, W.H. (1989) Measurements of sectional lift forces on a vibrating cylinder. Second Asia-Pacific Symposium on Wind Engineering, Beijing.

JONES, G.W. (1968) Unsteady lift forces generated by vortex shedding about a large, stationary, and oscillating cylinder at high Reynolds Numbers. Paper 687E-36, A.S.M.E. Symp. Unsteady Flow, Philadelphia.

SARPKAYA, T. (1978) Fluid forces on oscillating cylinders. A.S.C.E. J. Water. Port Coastal and Ocean Div., WW4, pp. 275-290.

VICKERY, B.J. and BASU, R.I. (1983) Across-wind vibration of structures of circular cross-section. Part 1. J. Wind Eng. and Ind. Aero., 12, pp. 49-73.

VICKERY, B.J. and CLARK, A.W. (1972) Lift or across-wind response of tapered stacks. A.S.C.E. J. Struct. Div., ST1, pp. 1-20.

Promotion of Instability During Lock-In

H.M. Blackburn
W.H. Melbourne
Monash University

Introduction

Lock-in is the phenomenon of phase-locking of vortex shedding to the oscillatory motion of slender cylindrical structures. The process by which this takes place is poorly understood, but the phenomenon is important in the design of slender, lightly damped structures such as steel chimney stacks and towers. This is because lock-in is associated with a form of aeroelastic instability which can lead to large amplitudes of cross flow motion for these kinds of structures. The instability mechanism can be thought of as a negative-damping type; in physical terms, vortex formation becomes correlated with the motion of the structure with a relative phase such that power is transferred to the structure from the passing air-stream. Large amplitudes of motion can result if the rate at which power is transferred to the structure exceeds the rate at which internal damping forces can dissipate it. Ultimately, the amplitude of motion is limited to about ± 1 diameter by non-linear aerodynamic effects.

Experimental Method

During an experimental programme conducted in the 450 kW wind tunnel at Monash University, cross flow (lift) forces which acted on short sections of a circular cylinder were measured. A feature of the equipment was that the cylinder could be forced to oscillate in a cross flow direction at amplitudes up to 3% of diameter. Since the frequency of oscillation could be varied, it was possible to vary the Reduced Velocity of oscillation ($V_r = U/fD$) while keeping the Reynolds number constant. The motion of the cylinder was measured using accelerometers installed within it.

Motion-Correlated Forces

As a part of the data reduction, lift forces which were correlated with the motion of the cylinder were calculated. Motion-correlated forces measured in smooth subcritical flow ($Re = 1.6 \times 10^5$, $I_u = 0.6\%$) showed the most interesting variation with Reduced Velocity and form the basis for discussion here. An important preliminary observation is that, even during lock-in, when the frequency of cylinder oscillation coincided with the vortex-shedding frequency, a large portion of the vortex shedding forces remained uncorrelated with motion.

The motion-correlated forces are presented here in the form of dimensionless coefficients: the Coefficient of Added Mass, C_a, and the Aerodynamic Damping Parameter K_a.

$$C_a = -C_{la} V_r^2 / 2\pi^3 \alpha$$

$$K_a = C_{lv} V_r^2 / 16\pi^2 \alpha$$

where C_{la} is the coefficient of lift correlated with cylinder acceleration and C_{lv} is the coefficient of lift correlated with cylinder velocity. The amplitude of oscillation occurs in the dimensionless form $\alpha = y_{\max}/D$. The Coefficient of Added Mass describes the acceleration-correlated

forces in terms of an equivalent mass of fluid, i.e.

$$l_a = -C_a \cdot \rho \frac{\pi D^2}{4} \cdot (2\pi f)^2 \cdot \alpha D$$

where l_a is the lift force correlated with cylinder acceleration per unit length. The Aerodynamic Damping Parameter is a form of mass-damping coefficient; for a uniform cylinder moving as a rigid body, an equivalent structural damping coefficient can be computed:

$$\zeta_{\text{aero}} = -K_a \frac{\rho D^2}{m}$$

where m is the mass per unit length of the structure. This shows that a positive value of K_a corresponds to *negative* damping, that is, the structure extracts power from the flow.

Values of C_a and K_a are shown as functions of Reduced Velocity in figure 1. During the measurements, the cylinder was forced to oscillate at a nominal amplitude $\alpha = 3\%$. As can be seen, there was a rapid change in the sign of K_a with change in V_r near $V_r = 5$ (this corresponds to a Strouhal number of 0.2). This change has been observed before, and has its physical basis in the change of phase of vortex shedding with respect to cylinder motion (see for example Zdravkovich 1982). More surprising were the high values of Coefficient of Added Mass observed near synchronization ($V_r = 5$), and the negative values observed at higher V_r. Again, there are precedents for the measurements (e.g. Nakamura, Kaku & Mizota 1971), but in this case the physical basis is less clear, although it may be associated with the formation of vortices at peak values of cylinder acceleration (as reported by Williamson & Roshko 1988).

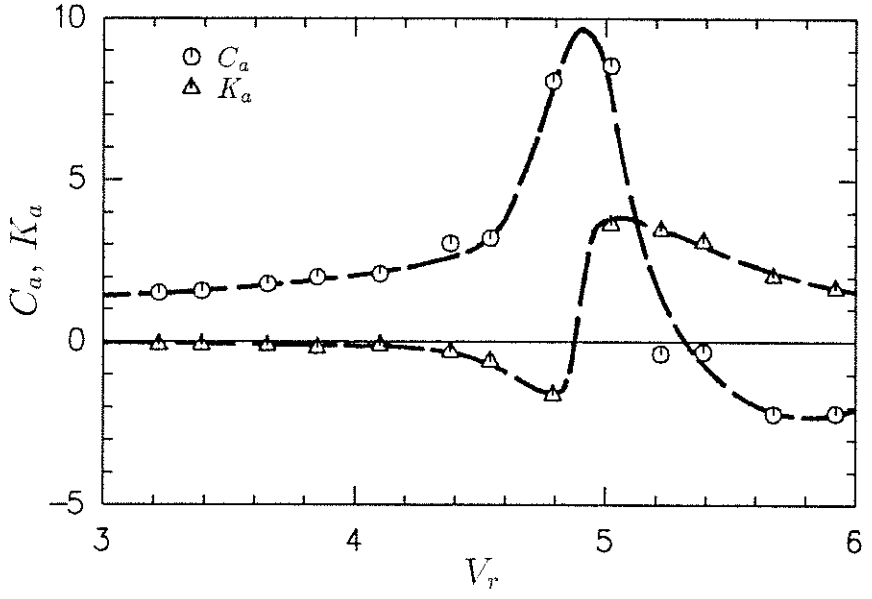

Figure 1: Values of Coefficient of Added Mass (C_a) and Aerodynamic Damping Parameter (K_a) as functions of Reduced Velocity (V_r).

Promotion of Instability

The results presented in figure 1 are replotted in polar form in figure 2, with V_r as a parameter. The asymptotic value of K_a as $V_r \to \infty$ is derived on a quasi-steady basis which gives

$K_a = -C_d V_r/8\pi$, where C_d is the Coefficient of Drag. As $V_r \to 0$ ($f \to \infty$), it is expected (and observed) that $C_a \to 1$, the value for a cylinder oscillating at small amplitude in stationary fluid.

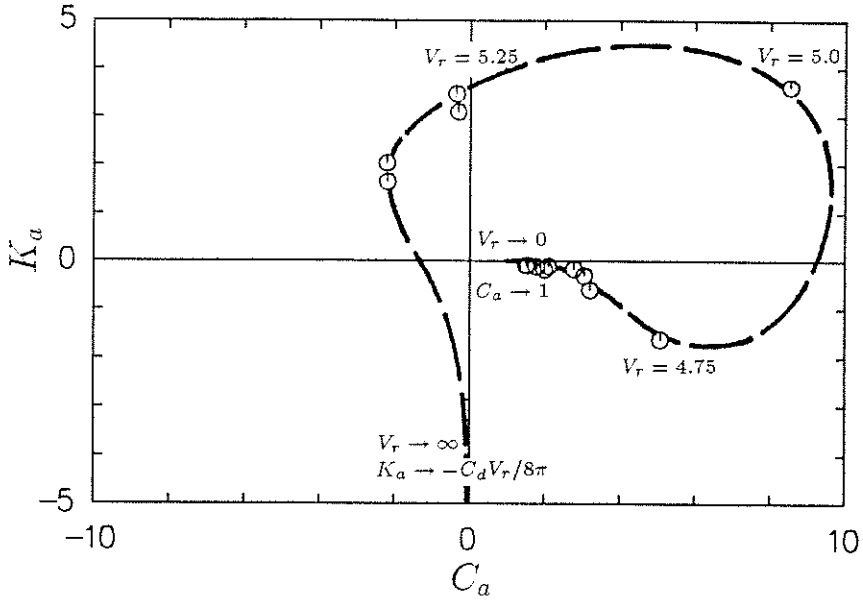

Figure 2: Values of Coefficient of Added Mass (C_a) and Aerodynamic Damping Parameter (K_a) in polar form with V_r as a parameter.

Instability, corresponding to positive values of K_a, is promoted near $V_r = 5$ by the following means. At $V_r > 5.25$, C_a is negative; this tends to increase the frequency of structural oscillation, thus decreasing the Reduced Velocity. Conversely, at $V_r < 5.25$, C_a is positive, which tends to reduce the frequency of structural oscillation, increasing V_r towards the zone of highest K_a.

To put the effect in perspective, the ratio of added mass to structural mass needs to be considered. For lightly-constructed steel chimney stacks, a typical ratio of structural mass per unit length to displaced mass of fluid per unit length is 50:1. This means that with $C_{a_{max}} \approx 10$, as shown here, the effective structural mass per unit length is reduced by about 20%.

References

Nakamura, Y., Kaku, S. & Mizota, T. 1971, 'Effect of mass ratio on the vortex excitation of a circular cylinder', *3rd Int. Conf. Wind Effects Build. & Struct.* Tokyo, pp. 727–36.

Williamson, C.H.K. & Roshko, A. 1988, 'Vortex formation in the wake of an oscillating cylinder', *J Fluids & Struct.* **2**, pp. 355–81.

Zdravkovich, M.M. 1982, 'Modification of vortex shedding in the synchronization range', *ASME J Fluids Eng.* **104**, pp. 513–17.

Lift on an Oscillating Cylinder in Smooth and Turbulent Flow

H.M. Blackburn and W.H. Melbourne

Department of Mechanical Engineering, Monash University, Clayton 3168, Australia.

Abstract

Lift forces were measured at six sections of a circular cylinder in smooth and turbulent flows over the Reynolds number range 1.1×10^5 to 5.5×10^5. Introduction of turbulence of 18% longitudinal intensity produced a return to organized vortex shedding, characterized by large lift forces with a broad spectral peak centred near $St = 0.23$. With the cylinder in forced oscillation of amplitudes up to 3% of diameter, motion-correlated forces were observed. Adaptive digital filter techniques were used to remove inertial components of force transducer signal.

1. INTRODUCTION

The prediction of amplitudes of cross wind vibration response of slender structures of circular cross section is one of the fundamental problems of Wind Engineering. Among the structures encompassed by this description are chimney stacks, masts and space-frame members. Typically, cross wind response amplitudes to vortex shedding must be limited to less than 5% of diameter in order to prevent the possibility of large amplitudes and stresses caused by lock-in effects.

For Reynolds numbers typical of structures and flows in Wind Engineering applications, vortex shedding is quasi-periodic, and prediction models are often based in random vibration theory, with estimates of mean-squared modal response amplitudes as the outcome. Models of this kind have been described by Vickery and Basu (1983), and the Engineering Sciences Data Unit in ESDU Item 85038. Both these models incorporate a description of vortex-induced lift forces on rigid cylinders in terms of the cross-spectra of lift acting at different points on the span and models of motion-correlated forces, which comprise an increasing proportion of lift force as oscillation amplitude increases. Both models give a coefficient of variation between predicted and observed response amplitudes of about 25% (Vickery & Basu 1984, ESDU 1985). A part of the variation can be attributed to a lack of data for the aerodynamic parameters which underly the models.

Only a limited amount of data are available to assist in the description of lift forces on rigid cylinders at transcritical Reynolds numbers, from a mixture of wind tunnel measurements made in smooth flows and a scattering of measurements conducted on full scale structures in turbulent flows. The extent of spanwise correlation of lift forces in transcritical flows has not been studied. In addition, the role of turbulence in establishing transcritical flows at comparatively low Reynolds numbers is poorly understood.

Motion-correlated forces referred to above are an aspect of the phenomenon of lock-in, in which it is observed that for large oscillation amplitudes, vortex shedding and structural oscillation become phase-locked, with the relative phase being a function of reduced velocity $V_r = U/fD$. At low amplitudes of oscillation it has been found that some proportion of lift force becomes correlated motion, with the remainder being uncorrelated over long

time periods (see e.g. Toebes & Ramamurthy 1967, Jones, Cincotta & Walker 1969). The consequences and nature of this partition of force into motion-correlated and uncorrelated components are poorly understood, although it has been implicit in many experiments in which lift forces on oscillating cylinders were measured.

These points served as motivation for a wind tunnel study of the local and spanwise distribution of lift force on a circular cylinder in smooth and turbulent flows ($I_{u_{max}} = 18\%$) over a range of Re up to 5.5×10^5. The model could be forced to oscillate cross flow at amplitudes up to $\pm 3\%$ of diameter, thus permitting study of the interaction of lift and motion in these flows.

2. WIND TUNNEL MODEL

2.1. Model geometry

A cylinder model was designed to suit the 2 m high, 1 m wide working section of the Monash University 450 kW wind tunnel. In a compromise between desires for high Reynolds number, low tunnel blockage and high aspect ratio, a cylinder geometry of 200 mm diameter and 900 mm length was selected, giving a blockage ratio of 10% and an aspect ratio of 4.5:1. While it is known that this combination of blockage and aspect ratio leads to over-estimates of force coefficients in smooth subcritical flow (see e.g. West & Apelt 1982), it is expected that the effect would be smaller in super- and transcritical flows, where the wake is narrower and the spanwise coherence of vortices is expected to be lower.

To minimize the effect of tunnel wall boundary layers on the measurements, large end plates were mounted 50 mm clear of the wind tunnel walls, with the cylinder spanning the 900 mm gap between them. The plates were rectangular, extending 2.5 D upstream, 4.5 D downstream of the cylinder centreline, 9 D cross flow. Since the model was designed to oscillate in the cross flow direction it was not attached to the end plates; a central supporting tube passed through holes in the end plates and the wind tunnel walls, with the clearance gap between the cylinder and the end plates sealed using synthetic fur, which allowed relative movement but prevented air flow through the gap.

The cylinder geometry is shown in figure 1, which indicates that the cylinder was constructed in segments, supported on an inner structural tube of 100 mm diameter. The thin (0.1 D axial length) cylinder segments contained lift force transducers, while the remainder were 'blank' segments that contained no instrumentation. The clearance gaps between the segments were sealed using narrow strips of 30 μm thick polyurethane elastomer, glued on. The use of six force transducers spaced along the span allowed measurements of lift force to be made simultaneously at the six locations. Since the lift transducers were narrow compared to typical lift force correlation lengths (order 1 D), the measurements obtained were assumed to be good approximations to the sectional lift forces.

2.2. Transducer construction

Transducer construction is illustrated in figure 2. The outer segments of the transducers were made as light as possible, consistent with the need for stiffness, by use of fibre composites, foamed plastics and balsa wood, giving a mass of 16 gm. Lift force was transmitted to the support cylinder by beam springs which had semi-conductor strain gauges bonded to them. The natural frequency of the outer segments on the springs was 400 Hz, well above the frequency content of the lift forces. Each transducer also contained an accelerometer for the measurement of cylinder motion and cancellation of inertial forces.

The mechanical arrangement of the springs and gauges provided sensor elements which

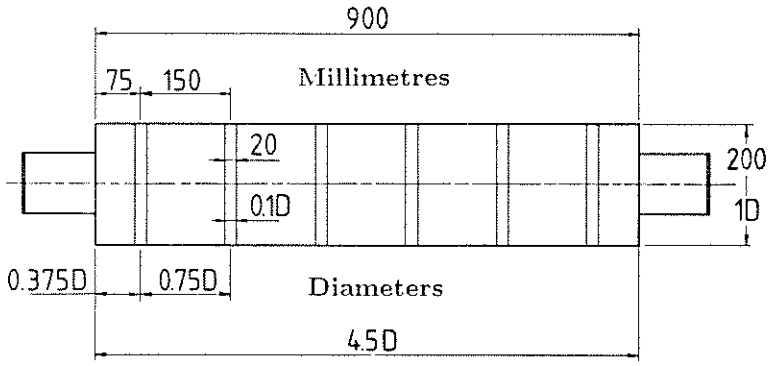

Figure 1: Cylinder geometry: six $0.1\,D/20$ mm long lift force transducers separated by 'blank' sections, all supported from an inner structural tube.

were sensitive only to lift force. Measurements showed the transducers to be about 150 times more sensitive to lift than to drag forces. The sensitivity to applied moments was also low; when cross flow force was applied at one cylinder radius from the centreline, strain bridge output changed by approximately 1/60th of the full reading obtained with the force centrally applied.

2.3. Oscillation system

The elements of the system can be seen in the sketch of figure 3. The system was designed to produce forced sinusoidal oscillations of up to $\pm 3\%\, D$ amplitude over a frequency range 10 Hz to 50 Hz. The part of the model described so far occupied the working section; outside this, it was supported and guided by a rectangular aluminium tube yoke and a harness of taut music wires which constrained motion to the cross flow direction. Underneath the tunnel floor, the yoke was clamped to two steel beam springs, and the assembly was driven at its resonant frequency by an electromagnetic shaker. The frequency could be adjusted by changing the length or section of the springs. A steel truss assembly held the shaker and the ends of the beam springs, and was clamped down to the main floor beams of the laboratory. Plenum boxes were used to surround the wire harness and the cylinder ends where they penetrated the working section walls. The yoke struts passed through the lower faces of the boxes, with a small clearance limiting the flow of air into the working section.

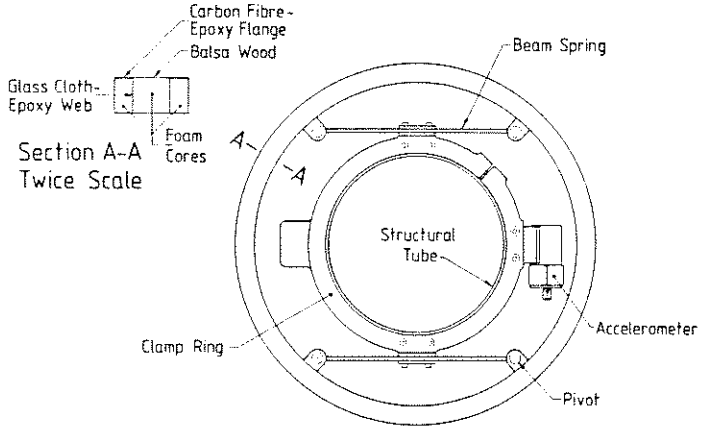

Figure 2: End view of lift force transducer station, showing construction. A full bridge of semiconductor strain gauges were bonded to the beam springs.

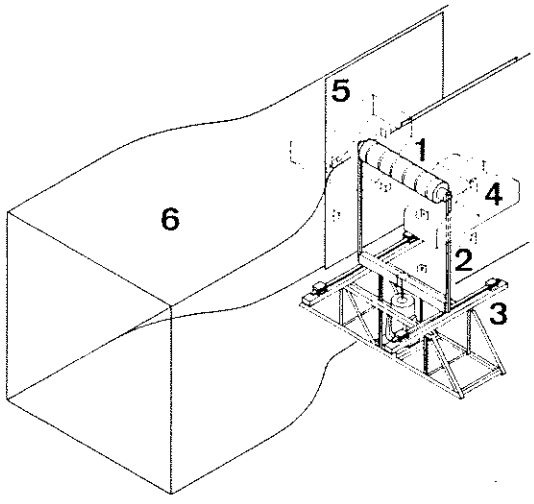

Figure 3: Sketch of cylinder installed in wind tunnel. **1**: Cylinder with six force transducers; **2**: Driving yoke and wire harness; **3**: Support truss, springs and electromagnetic shaker; **4**: Plenum box; **5**: End plate; **6**: Contraction.

3. FLOW

Five turbulence configurations were selected. Smooth flow was obtained using a combination of wire meshes and an aluminium honeycomb screen, while turbulent flow was produced using a bi-planar array of slats located upstream of the contraction. The spanwise average values of the longitudinal and transverse turbulence intensities (I_u & I_v), together with the turbulence integral length scales are shown in table 1.

Table 1: Spanwise-averaged turbulence intensities and integral scales at the model centreline position for the five flow configurations.

Configuration	I_u%	I_v%	L_u^x/D
1	18.0	14.1	0.53
2	9.6	8.7	0.53
3	4.2	4.2	0.50
4	3.6	3.6	0.25
'Smooth Flow'	0.6	0.6	0.10

The close agreement between I_u and I_v, except for the highest intensity case, indicates that the turbulence was approaching isotropy after distortion caused by the contraction. For Configuration 1, differing longitudinal and transverse intensities (I_u = 18%, I_v = 14%) indicate that the turbulence was still approaching isotropy, but it was felt that the high values, similar to those found in many full scale applications, made its inclusion worthwhile.

Turbulence integral scales L_u^x were obtained by fitting von Kármán spectra to the measured velocity spectra.

4. SIGNAL PROCESSING

Signals from the transducers (six accelerometers, six strain bridge amplifiers) were low-pass filtered, then digitized and stored on magnetic tape using a minicomputer. All subsequent signal processing was carried out digitally.

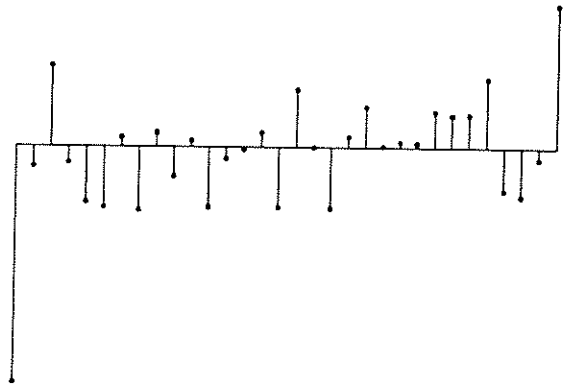

Figure 4: Typical impulse response function of a digital filter used for cancellation of inertial signal.

4.1. Inertial signal cancellation

When the cylinder was oscillating, forces due to the mass and acceleration of the transducer outer segments were produced, in addition to aerodynamic forces. Adaptive digital filter techniques described by Bellanger (1987) were used to identify the relationship between accelerometer outputs and strain bridge signals found when the cylinder was forced to oscillate without flow. An example of a digital filter produced by this technique is illustrated in figure 4. To remove the inertial component of force transducer output in the presence of flow, the accelerometer signals were convolved with the digital filters and the result subtracted from the total force transducer signals, leaving aerodynamic forces as residual. An example of force transducer signal before and after removal of inertial force component is shown in figure 5.

To check the accuracy of the cancellation method, tests were run in which data for both the identification and measurement phases were recorded without flow. The removal of inertial signal typically left a residual with RMS magnitude less than one analogue to digital conversion level (5 mV). When flow was applied, the typical RMS level of the aerodynamic force signal was 0.5 V, giving a signal to noise ratio of approximately 40 dB.

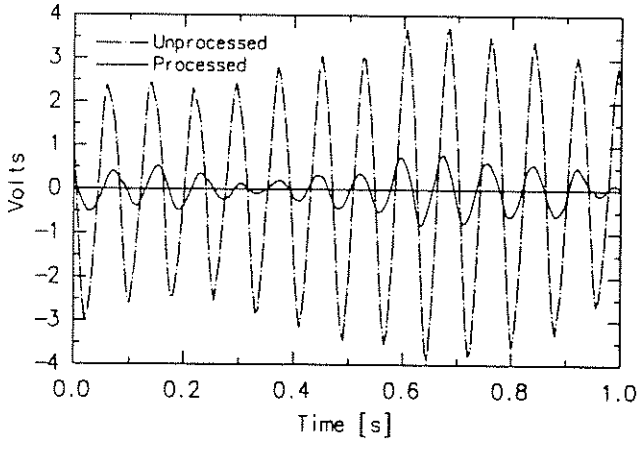

Figure 5: Example of transducer signal obtained in smooth subcritical flow, before and after removal of inertial signal component.

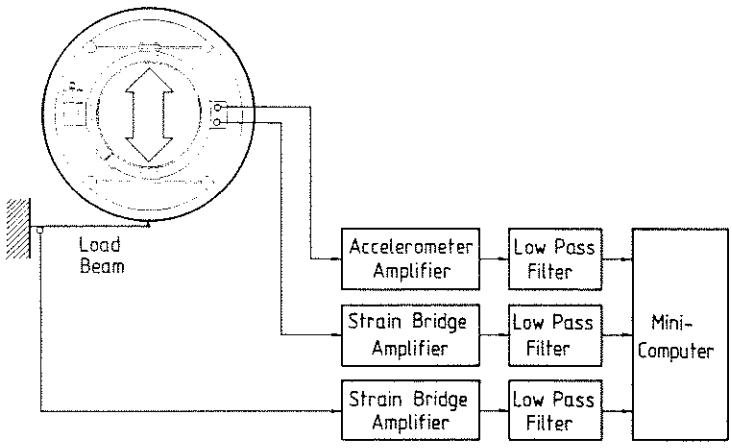

Figure 6: Schematic of equipment set-up for dynamic calibration of force transducer. Transducer forced to oscillate cross flow while in contact with load beam.

4.2. Re-introduction of 'added mass' forces

Although the cancellation system effectively removed all forces due to the acceleration of the transducer segment mass, it is known from both theory (Milne-Thomson 1960) and measurements (Lundgren et al. 1979) that 'added mass' forces per unit length equivalent to accelerating the mass per unit length of one cylinder's cross-section of fluid exist at small oscillation amplitudes in still fluid. These forces were also cancelled using the system described above, so forces of the appropriate magnitude were subsequently calculated with the aid of the accelerometer timeseries, and added back to the force transducer signals. While viscous forces proportional to cylinder velocity must also have arisen when the cylinder oscillated in still fluid, it can be shown with the use of theoretical results for oscillatory boundary layers (Batchelor 1967) that at the cylinder Reynolds numbers for oscillation in still fluid, the resulting viscous forces were small enough to lie within the noise level of the measurements, and so were ignored.

4.3. Integration of accelerometer timeseries

Since both velocity and acceleration of the cylinder were required for subsequent analysis of results, the cylinder acceleration timeseries were integrated to obtain velocity timeseries. In order to avoid phase errors inherent in typical numerical integration formulae, a numerical integration procedure was devised in which DFT coefficients were manipulated in the frequency domain (effectively by dividing them by $j2\pi f$). Data were then returned to the time domain for further processing.

4.4. Dynamic calibration

It was found that the polyurethane film used to seal the clearance gaps between the transducer and 'blank' cylinder segments had slightly viscoelastic properties. Upon application of a steady load to a transducer, strain bridge amplifier output would jump nearly instantaneously to about 90% of its full value, then relax slowly to the full value over a period of several minutes. It was established experimentally that over the frequency range of interest (5 Hz to 150 Hz), the effect was almost purely elastic.

In response, a dynamic calibration procedure was devised. The layout of the equipment is illustrated in figure 6. The method relied on applying a fluctuating force to the force

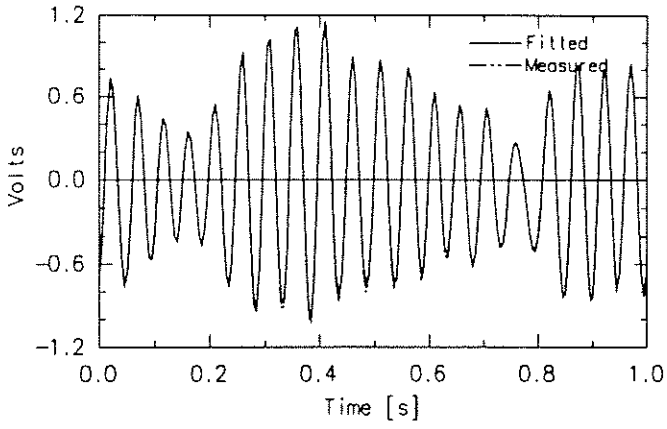

Figure 7: Dynamic calibration: after removal of inertial signal, amplitude of residual transducer output was fitted to match measured load beam signal.

transducer segment, using a pre-calibrated lightweight steel load beam.

Calibration proceeded as follows. First, the model was forced to oscillate without the load beam, and data collected from the transducer strain gauge bridge and accelerometer amplifiers. These data were used to identify the digital filter which related acceleration and inertial transducer response. Then the load beam was pre-loaded against the transducer segment with sufficient deflection that it would not lose contact when the cylinder was oscillated. The cylinder was forced to oscillate again, and outputs from the three amplifiers (load beam and transducer strain bridges, transducer accelerometer) were recorded. Next, the inertial component of force transducer output was estimated by convolution of the digital filter with the accelerometer signal, and subtracted to leave a remainder due to the force applied by the load beam. Finally, this remainder was scaled to match the load beam signal using a least-squares fit. The resulting scale factor was multiplied by the load beam force-voltage calibration factor to produce a calibration for the transducer strain bridge.

Advantages of the method were that it provided a cross-check on the inertial signal removal technique, and enabled the force measurement procedure to be checked under simulated experimental conditions. An example of part of the calibration procedure is shown in figure 7, where the fitted residual transducer signal is shown with the signal from the load beam.

5. RESULTS

5.1. Plan of experiments

It was decided to first carry out a series of experiments in which the model was held fixed and the range of achievable Reynolds numbers was traversed for each of the five flow configurations.

With the oscillation system described above, it was possible to vary the Reynolds number $Re = UD/\nu$ and the reduced velocity $V_r = U/fD$ independently, since the frequency of oscillation could be readily changed. Traverses of reduced velocity ($3 < V_r < 6$) were carried out at each end of the Reynolds number envelope ($1.1 \times 10^5 < Re < 5.5 \times 10^5$) with the aim of studying the interaction of motion and lift both in smooth subcritical flow and in turbulent transcritical flows. Amplitudes $\alpha = y_{max}/D = 1\%$, 2% and 3% were used.

Due to uncertainty about blockage correction at these Reynolds numbers, none was applied.

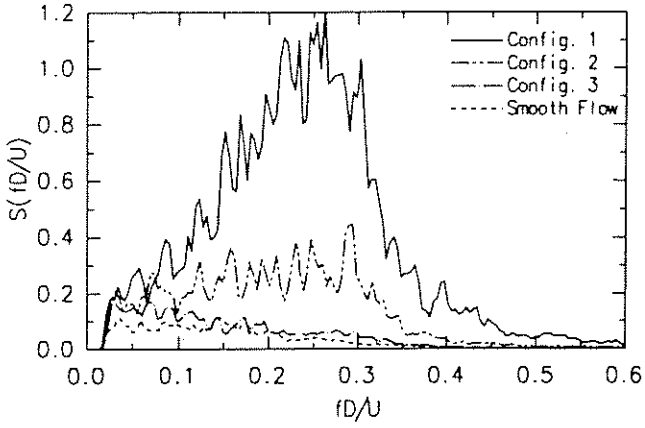

Figure 8: Influence of turbulence configuration on sectional lift force spectra at $Re \approx 4.6 \times 10^5$. Spectra are normalized such that their areas equal the mean-squared coefficients of sectional lift force.

5.2. Effect of turbulence

With the cylinder held fixed in smooth flow, it was found that the critical transition occurred at $Re \approx 2.3 \times 10^5$. At higher Reynolds numbers, no distinct peak was observed in the lift force spectra, with spectral densities decreasing monotonically from maxima at low frequencies.

Introduction of low intensity turbulence (Configs. 3 & 4) produced critical transition at lower Reynolds numbers, as expected. Above transition, lift force spectra and variances were very similar to those observed in smooth flow.

For the two highest turbulence intensities (Configs. 1 & 2), critical transition occurred at Reynolds numbers below the minimum attainable in the experiment. for each intensity, there was only a comparatively slight change in properties of lift with Reynolds number over the range investigated. The change in properties of lift with turbulence intensity, however, was pronounced. At the highest intensity ($I_u = 18\%$), a clear but very broad peak existed in the lift force spectra, centred around $St = fD/U = 0.23$. RMS sectional lift was approximately three times greater than in smooth flow. In addition, the spanwise correlation of lift increased above that in the supercritical flows at lower Reynolds numbers. The second highest intensity produced results between those for the lower intensities and the highest, with intermediate RMS sectional lift and some evidence of a peak in the lift force spectra.

The influence of turbulence intensity is clearly shown in the comparison of spectra of sectional lift for four of the five turbulence configurations, all recorded at $Re \approx 4.6 \times 10^5$, presented in figure 8.

5.3. Motion-correlated forces in subcritical smooth flow

When the cylinder was forced to oscillate cross flow, it was found, as in other experiments (e.g. Toebes & Ramamurthy 1967, Jones, Cincotta & Walker 1969) that some proportion of lift force could be correlated with cylinder motion over extended time periods. In this experiment, the amount of force correlated with motion was estimated by extracting least-squares fits of lift force timeseries to cylinder acceleration and velocity timeseries. The residual force timeseries was thus uncorrelated with motion on a least-squares basis. This processing is the digital equivalent of analogue procedures which have been applied in the past, for example by Jones, Cincotta and Walker. An example of this process is shown in figure 9, where the decomposition just described is illustrated, with velocity- and acceleration-correlated force timeseries extracted from the total to leave a residual uncorrelated timeseries of lift coefficient.

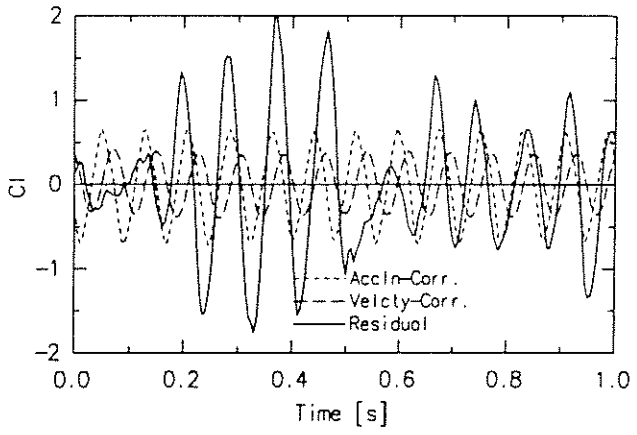

Figure 9: Sectional coefficient of lift in smooth subcritical flow decomposed into parts equivalent to the long-time-average acceleration- and velocity-correlated forces, with residual uncorrelated force.

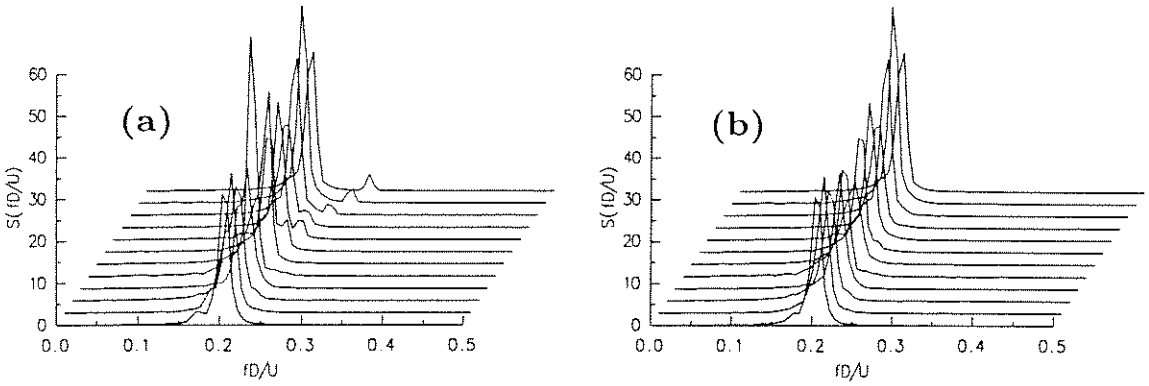

Figure 10: Spectra of sectional lift forces in smooth subcritical flow, showing the relative contribution of motion-correlated forces with the cylinder oscillating near the critical reduced velocity, with amplitude $\alpha = 3\%$. **a**: Spectra prior to extraction of motion correlated force components; **b**: Spectra of residual forces.

Lift spectra An examination of the spectra of total lift forces shows that two peaks are often visible, one at the frequency of cylinder oscillation, the other at the Strouhal frequency (fig. 10(a)). After extraction of motion-correlated terms from the timeseries of force, the associated spectra reveal that the peaks at the cylinder oscillation frequencies have been removed (fig. 10(b)). It can be seen, as for the timeseries of lift in figure 9, that the motion-correlated lift makes only a small contribution to the total lift force at these amplitudes of motion.

Force coefficients The motion-correlated coefficients of lift extracted by the procedure described above have been converted to force coefficients C_a and K_a for the acceleration- and velocity-correlated lift respectively. In these forms they are more directly comparable with structural mass and damping.

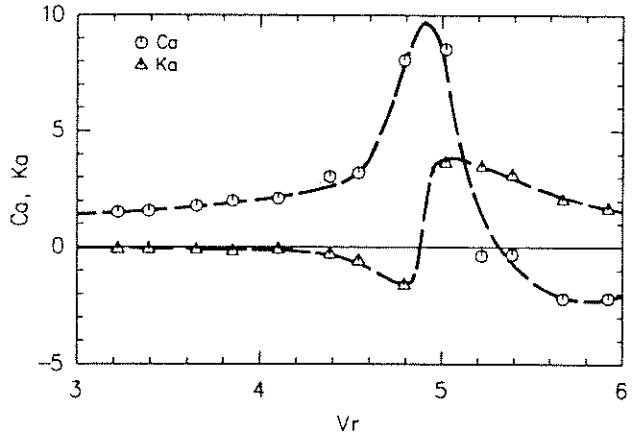

Figure 11: Variation with reduced velocity V_r of coefficients C_a and K_a of motion-correlated forces in smooth subcritical flow. $Re \approx 1.6 \times 10^5$, $\alpha \approx 3\%$.

The *coefficient of added mass*, C_a, describes the acceleration-correlated force per unit length, l_a, as a proportion of the force per unit length required to accelerate the mass of fluid displaced by the cylinder:

$$l_a = -C_a \cdot \rho \frac{\pi D^2}{4} \cdot \ddot{y}$$

The velocity-correlated force per unit length, l_v, is described in terms of an *aerodynamic damping parameter*, K_a.

$$l_v = K_a \cdot 16f \cdot \rho \frac{\pi D^2}{4} \cdot \dot{y}$$

Here, the term $K_a \cdot 16f \cdot \rho\pi D^2/4$ has the same dimensions and form as a coefficient of structural damping per unit length. For convenience of comparison, an equivalent structural damping ratio can be computed; for a uniform cylinder with mass per unit length m, oscillating with a uniform mode shape,

$$\zeta_{\text{aero}} = -K_a \frac{\rho D^2}{m}$$

The variation in smooth subcritical flow of C_a and K_a with reduced velocity V_r for $\alpha = 3\%$ is shown in figure 11. The rapid variation of C_a and K_a near the critical reduced velocity $V_r \approx 5$ is apparent; this represents a change in phase angle of the motion-correlated forces with respect to cylinder motion.

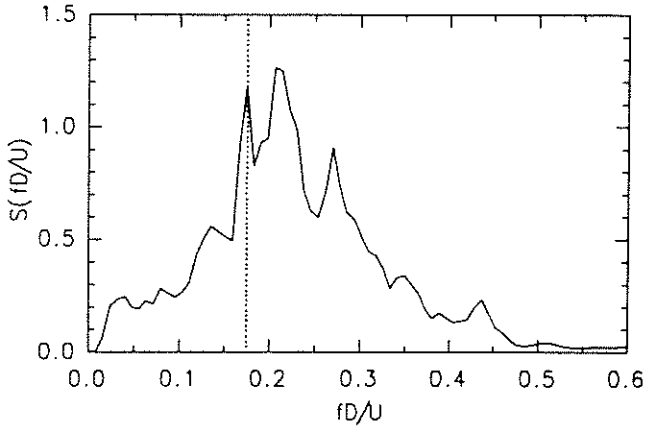

Figure 12: Spectrum of sectional lift with cylinder oscillating in turbulent flow (config. 1, $I_u = 18\%$); $Re \approx 4.6 \times 10^5$, $\alpha \approx 3\%$. Dotted line indicates frequency of oscillation.

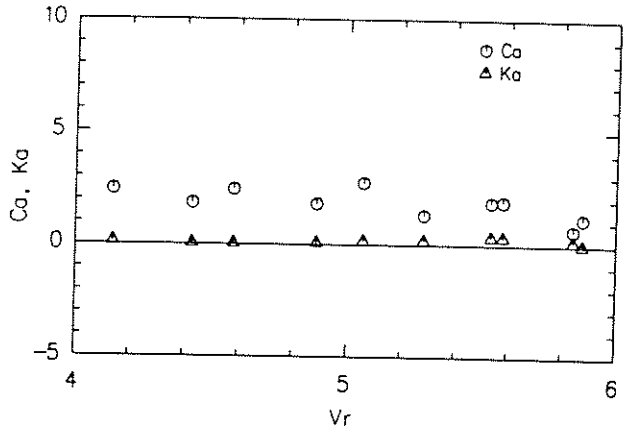

Figure 13: Variation with reduced velocity V_r of coefficients C_a and K_a of motion-correlated forces in turbulent transcritical flow, $I_u = 18\%$. $Re \approx 4.6 \times 10^5$, $\alpha \approx 2\%$.

5.4. Motion-correlated forces in transcritical turbulent flow

Motion-correlated forced were observed for all Reynolds numbers and flow configurations, but in general the magnitudes were smaller than in subcritical smooth flow, and the magnitudes and phases with respect to motion of the forces showed more scatter and little influence of reduced velocity.

An example of a lift force spectrum from one transducer in the $I_u = 18\%$ turbulence configuration with $Re = 4.6 \times 10^5$ is shown in figure 12, while the variation of C_a and K_a with V_r for this flow are given in figure 13.

6. DISCUSSION

As has been known for many decades, smooth flows with Reynolds numbers in the range available in this experiment ($1.1 \times 10^5 < Re < 5.5 \times 10^5$), produce both subcritical and supercritical behaviour, while introduction of turbulence brings about the critical transition at lower Reynolds numbers. It has been anticipated that turbulence would also promote the appearance of transcritical flow at lower Reynolds numbers than in smooth flow (see e.g. Zdravkovich 1990). The results presented here for the two highest turbulence intensities support this view; in particular the lift force spectrum for $I_u = 18\%$, which has a broad spectral peak centred at $St = 0.23$, indicates that strong vortex shedding was re-established at $Re = 4.6 \times 10^5$, despite the disruptive influence of turbulence.

The measurements of lift on the oscillating cylinder in subcritical smooth flow show similar characteristics to previous measurements obtained in smooth flows. The rapid variation in motion-correlated force near the critical velocity is probably associated with a change in phase of motion-correlated vortex shedding with respect to cylinder motion, as indicated by previous flow-visualization experiments (see Zdravkovich 1982). It should be emphasized that the force coefficients for motion-correlated forces represent time-averaged values and do not imply, as may be suggested by figure 9, that steadily-fluctuating motion-correlated forces exist during each cycle of cylinder motion.

The measurements of motion-correlated forces obtained in turbulent transcritical flow are significant for the design of full scale structures in Wind Engineering applications. The scatter in the results probably reflects the fact that vortex shedding was less well-organized than for the subcritical smooth flow. The absence of any clear trend of motion-correlated forces with V_r is also likely to be a reflection of this lack of organization. Average values of motion-correlated force coefficients suggest that long-time-average values are likely to be small in these flows. Taken overall, the results for $I_u = 18\%$, $Re = 4.6 \times 10^5$ suggested slight positive values for K_a, of order 0.2.

7. CONCLUSIONS

In many experiments in which the objective is to measure loads on oscillating structures, it is necessary to cancel out transducer signals which are caused by motion of the structure, so that fluid-induced forces or pressures may be analysed separately. Adaptive digital filter techniques were shown to be well suited to the task.

On the evidence of a broad but well-defined peak in the spectra of lift force, high intensity turbulence promoted transition to transcritical flow at Reynolds numbers which would produce supercritical behaviour in smooth flow. The broadness of the peak reflects the fact that vortex shedding was poorly organized when compared to smooth subcritical and transcritical flows.

Introduction of forced cross-flow oscillation produced motion-correlated lift forces. In smooth subcritical flow, variation of these forces with reduced velocity was similar to that observed in previous experiments, with rapid variation near the critical reduced velocity. Examination of the spectra of lift force produced before and after removal of motion-correlated forces showed that removal of motion-correlated forces also removed spectral peaks at frequencies of cylinder oscillation.

Motion-correlated forces in transcritical turbulent flows showed a good deal of scatter and small average values.

8. REFERENCES

Batchelor, G.K., 1967, *An Introduction to Fluid Dynamics*, Cambridge University Press.

Bellanger, M., 1987, *Adaptive Digital Filters and Signal Analysis*, Marcel Dekker.

Engineering Sciences Data Unit, 1985, *Item 85038: Circular-Cylindrical Structures: Dynamic Response to vortex shedding. Pt. 1: Calculation Procedures and Derivation.*

Jones, G.W., Cincotta, J.J. & Walker, R.W., 1969, 'Aerodynamic forces on a stationary and oscillating cylinder at high Reynolds numbers', *NASA TR R-300.*

Lundgren, H., Brink-Kjær, O., Sand, S.E. & Jacobsen, V., 1979, 'Improved physical basis of wave forces', *ASCE Proc. Spec. Conf. Civ. Eng. in Oceans IV*, Vol. 1., San Francisco.

Milne-Thomson, L.M., 1960, *Theoretical Hydrodynamics*, 4th ed., MacMillan.

Toebes, G.H., & Ramamurthy, A.S., 1967, 'Fluidelastic forces on circular cylinders', *ASCE J Eng. Mech. Div.*, EM6, pp. 1–20.

Vickery, B.J., & Basu, R.I., 1983, 'Across-wind vibration of structures of circular cross section. Pt. 1: Development of a mathematical model for two-dimensional conditions', *J Wind Eng. Ind. Aero.*, **12**, pp. 49–73.

Vickery, B.J., & Basu, R.I., 1984, 'The response of reinforced concrete chimneys to vortex shedding', *Eng. Struct.*, **6**, pp. 324–333.

West, G.S., & Apelt, C.J., 1982, 'The effects of tunnel blockage and aspect ratio on the mean flow past a circular cylinder with Reynolds numbers between 10^4 and 10^5', *J Fluid Mech.*, **114**, pp. 361–377.

Zdravkovich, M.M., 1982, 'Modification of vortex shedding in the synchronization range', *ASME J Fluids Eng.*, **104**, pp. 513–517.

Zdravkovich, M.M., 1990, 'Conceptual overview of laminar and turbulent flows past smooth and rough circular cylinders', *J Wind Eng. Ind. Aero.*, **33**, pp. 53–62.